



Controlling hydrogenation of C=O and C=C bonds in cinnamaldehyde using silica supported Co-Pt and Cu-Pt bimetallic catalysts

Renyang Zheng^a, Marc D. Porosoff^b, Jacob L. Weiner^b, Shuliang Lu^a, Yuexiang Zhu^{a,**},
Jingguang G. Chen^{b,*}

^a Beijing National Laboratory for Molecular Sciences, State Key Laboratory for Structural Chemistry of Unstable and Stable Species, College of Chemistry and Molecular Engineering, Peking University, Beijing 100871, China

^b Department of Chemical Engineering, Center for Catalytic Science and Technology, University of Delaware, Newark, DE 19716, USA

ARTICLE INFO

Article history:

Received 7 November 2011

Received in revised form 9 January 2012

Accepted 15 January 2012

Available online 25 January 2012

Keywords:

Hydrogenation

Cinnamaldehyde

Bimetallic Catalysts

Co-Pt

Cu-Pt

ABSTRACT

Liquid phase hydrogenation of cinnamaldehyde was evaluated over SiO₂ supported Co-Pt and Cu-Pt bimetallic and Co, Cu, Pt monometallic catalysts in a batch reactor. H₂-temperature-programmed reduction (H₂-TPR) was utilized to characterize the reduction behavior and pulse CO chemisorption measurement was performed to characterize the number of active sites of the catalysts. Transmission electron microscopy (TEM) analysis was used to characterize metallic particle size distribution and extended X-ray absorption structure (EXAFS) measurements were performed to verify the bimetallic bond formation. The reactor evaluation results show that Co-Pt and Cu-Pt bimetallic catalysts exhibit much higher hydrogenation activity than the corresponding monometallic catalysts, and Co-Pt shows much higher selectivity toward C=O bond hydrogenation than Cu-Pt. The trend of hydrogenation activity and selectivity is consistent with previous studies of the hydrogenation of unsaturated aldehydes on model bimetallic surfaces.

© 2012 Elsevier B.V. All rights reserved.

1. Introduction

Selective hydrogenation of α,β -unsaturated aldehydes to the corresponding allylic alcohols has received considerable attention because of its industrial applications [1–3]. The competing hydrogenation pathways of α,β -unsaturated aldehydes can occur through the C=C bond to produce the saturated aldehydes and the carbonyl group to produce unsaturated alcohols. Hydrogenation of the C=C bond is thermodynamically more favorable, and hence research efforts have been directed at improving the selectivity to the more desirable unsaturated alcohols [4]. Many attempts have been made to promote the selective hydrogenation of α,β -unsaturated aldehydes by taking advantage of the synergistic effects of bimetallic catalysts [5–17], such as Co-Pt [5–8], Fe-Pt [9], Ru-Pt [10,11], and Sn-Pt [12]. The catalytic activity and selectivity are influenced by several factors, including reaction conditions and operation mode (e.g. gas or liquid phase hydrogenation), electronic and geometric structures of the metal catalysts, type of catalyst supports, and catalyst preparation and activation procedures.

In order to better understand the hydrogenation pathways of α,β -unsaturated aldehydes on bimetallic catalysts, fundamental studies on Pt single crystal and Pt-based bimetallic surfaces have been performed by adding a 3d-metal, such as Fe, Co, Ni and Cu, to Pt(1 1 1) [18,19]. The 3d-Pt bimetallic catalysts often show properties that differ distinctly from those of their parent metals, offering the opportunity to obtain novel catalysts with enhanced activity and/or selectivity [20–22]. For example, it has been demonstrated under ultra-high vacuum (UHV) conditions that a Pt-terminated Pt-Co-Pt(1 1 1) surface, which represents a subsurface bimetallic structure with Pt on the top-most surface layer and Co residing in the subsurface region, promoted the selective hydrogenation of acrolein (CH₂=CH–CH=O) toward the corresponding unsaturated alcohol [19]. The combined experimental and DFT results suggested that the presence of weakly adsorbed acrolein through a di- σ -C–O configuration appeared to be responsible for this desired hydrogenation pathway [19].

More recently, these surface science results have been extended to γ -Al₂O₃ supported Co-Pt bimetallic catalysts, which exhibit significantly higher activity than monometallic Co and Pt catalysts for the hydrogenation of C=O bonds in two probe molecules, acetone and acetaldehyde [23]. In the current work we extended the hydrogenation of monocarbonyl compounds to that of α,β -unsaturated aldehydes on silica supported Co-Pt bimetallic catalysts. In addition, Cu-Pt catalysts were also evaluated due

* Corresponding author. Tel.: +1 302 831 0642; fax: +1 302 831 1048.

** Corresponding author.

E-mail addresses: zhuyx@pku.edu.cn (Y. Zhu), jgchen@udel.edu (J.G. Chen).

to its selectivity in the partial hydrogenation of butadiene [24] and 1,4-cyclohexadiene [25]. Several characterization methods, including H₂-temperature-programmed reduction (H₂-TPR), pulse CO chemisorption, transmission electron microscopy (TEM) and extended X-ray absorption fine structure (EXAFS), were employed in order to understand the catalytic behavior and bimetallic effects. Because of the toxicity of acrolein, cinnamaldehyde (CMD) was used as the probe molecule in the current work to identify the selective hydrogenation pathways on the bimetallic catalysts. From the point of view of practical applications, the corresponding semi-hydrogenated product, cinnamyl alcohol (CML), is utilized as components in pharmaceuticals, fragrances, and perfumes [4,26].

2. Experimental methods

2.1. Catalyst preparation

A slurry-based impregnation method was used to prepare the 5.0 wt%Co–1.7 wt%Pt/SiO₂ and 5.4 wt%Cu–1.7 wt%Pt/SiO₂ bimetallic catalysts, with a Co:Pt (or Cu:Pt) metal atomic ratio of 10:1. The corresponding monometallic Co, Cu and Pt catalysts were also prepared to serve as control samples.

The silica gel was first calcined at 1073 K for 3 h to obtain the thermally stable silica support, with a BET specific surface area of 370 m² g⁻¹ and a total pore volume of 0.84 cm³ g⁻¹. The metal precursors were dissolved in an excess of deionized water (15 mL H₂O per gram of catalyst) and then impregnated into the silica support. The solution was sonicated for 1 h, then dried at 373 K for 24 h, and finally calcined at 623 K for 2 h. The metal precursors used in this study were Co(NO₃)₂·6H₂O, Cu(NO₃)₂·3H₂O, and Pt(NH₃)₄(NO₃)₂ (A.R.).

2.2. Catalyst characterization

2.2.1. H₂-temperature-programmed reduction (H₂-TPR)

TPR experiments were performed to determine the reduction behavior of the catalysts. The experiments were carried out in a U-shaped tubular quartz reactor heated by an electric furnace. For each measurement, 0.040 g of calcined catalyst (40–80 mesh) was exposed to a reducing gas consisting of 5.0 vol% H₂ in Ar (10 mL min⁻¹) with a temperature ramp from room temperature to 1073 K at 10 K min⁻¹. The amount of hydrogen consumption was detected by a thermal conductivity detector (TCD).

2.2.2. CO chemisorption

Pulse CO chemisorption was performed using a Micromeritics AutoChem II 2920 to determine the number of active sites on the surfaces of the reduced catalysts. Approximately 0.05 g of the catalyst was reduced by 30 mL min⁻¹ 10 vol.% H₂ in He at 623 K (723 K for monometallic Co catalyst) for 1.5 h, and then held for 2 h in He. After cooling in He, gas pulses consisting of 5.0 vol.% CO in He were injected at 50 mL min⁻¹ at 308 K and the signal was monitored using a TCD.

2.2.3. Transmission electron microscopy (TEM)

TEM analysis was performed on pre-reduced catalysts using a JEOL 2010F equipped with a Schottky field emission gun operated at 200 keV, with an ultra-high resolution pole piece providing a point resolution of 1.9 Å. Imaging analysis was performed in the scanning mode (STEM) using a 12 nm camera length and a 1.0 nm diameter nanoprobe. TEM samples were prepared by grinding and suspending reduced catalysts in ethanol, and then a few droplets of this solution were placed onto a carbon-coated copper grid. The grids were allowed to fully dry before loading the samples into the TEM.

2.2.4. Extended X-ray absorption fine structure (EXAFS)

EXAFS experiments were performed on the X18B beamline at the National Synchrotron Light Source (NSLS), Brookhaven National Laboratory. The sample preparation procedures have been previously reported [27]. The catalysts were reduced under a diluted hydrogen flow (5% H₂ in He, 40 mL min⁻¹) while heating to 623 K at a rate of 10 K min⁻¹. The samples were held at 623 K for 1 h and then allowed to cool to room temperature at 10 K min⁻¹ under a diluted H₂ flow. The Pt L_{III}-edge EXAFS spectra were then collected at room temperature using a double crystal Si(1 1 1) monochromator. EXAFS measurements were also collected from a Pt foil in order to calibrate the edge energies of the catalyst samples.

The EXAFS spectrum was analyzed using the IFFEFIT 1.2.11 data analysis package (Athena, Artemis, Atoms, and FEFF6) [28,29]. Local structural information was obtained by using Artemis to fit each data set with theoretical standards generated by FEFF6 in R-space [30]. For each catalyst the Pt–Pt and the Pt–3d (3d = Co or Cu) contributions to the theoretical EXAFS were taken into account in fitting the data for the bimetallic catalysts, while only Pt–Pt contributions were included in fitting the monometallic Pt catalyst. The theoretical Pt–Pt photoelectron amplitudes and phases were calculated for the bulk Pt fcc structure. The Pt–3d contributions were calculated using the same Pt fcc structure with the exception that the Pt atoms in the first nearest-neighbor shell were replaced with Co or Cu atoms. The passive electron reduction factor (S_0^2) was found to be 0.80 from fitting of the Pt-foil data, and this value was fixed through the fitting of all the catalysts. The seven parameters used in the fitting procedure were the correction to the edge energy, the coordination numbers of the Pt–Pt and Pt–3d bonds, corrections to their model interatomic distances, and the mean square deviations in interatomic distances (EXAFS Debye–Waller factors).

2.3. Catalytic evaluation

The catalytic hydrogenation reaction was performed in a stainless steel stirred autoclave with a volume of 100 mL. In a typical experiment, 0.100 g catalyst was reduced in a U-shaped quartz tube under a H₂ (20 mL min⁻¹) and N₂ (20 mL min⁻¹) mixture at 623 K (723 K for monometallic Co catalyst) for 1 h and then cooled to room temperature. To prevent air contact of the freshly reduced catalyst powder, about 3 mL isopropanol (solvent) was dropped into the tube to immerse the catalyst under the H₂/N₂ mixture. Then the isopropanol immersed catalyst was transferred carefully to the autoclave, including 26 mL isopropanol and 3 mL CMD. The total volume of reactant and solvent was 27 mL. After the autoclave was sealed, H₂ was charged four times to replace air and the initial pressure of H₂ was 0.5 MPa. The autoclave was heated to the reaction temperature of 353 K in 0.5 h and H₂ was charged to a final pressure of 4.0 MPa. The hydrogenation reaction began by starting the stirring mechanism. After the desired reaction time, the stirring was cut off, and the autoclave was quickly cooled to room temperature and depressurized, and about 0.3 mL liquid samples were collected periodically. The liquid samples were analyzed on a gas chromatography (GC) equipped with a flame ionization detector (FID).

3. Results

3.1. H₂-TPR

The reduction behavior of the calcined catalysts by TPR is shown in Fig. 1. The Co/SiO₂ shows two main reduction peaks close to each other with temperature maxima at about 590 K and 630 K. The first peak is assigned to the reduction of Co₃O₄ to CoO, and the second

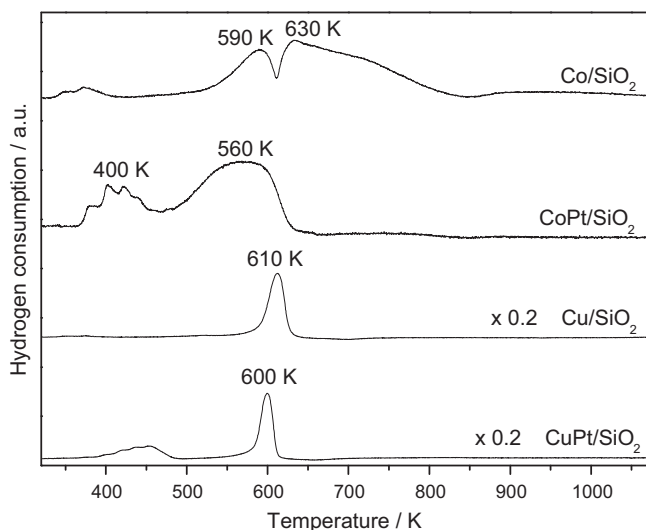


Fig. 1. TPR profiles of the calcined Co-Pt and Cu-Pt bimetallic and corresponding monometallic catalysts supported on silica.

one to the subsequent reduction of CoO to metallic Co [31,32]. The detection of the tail or shoulder reduction peak around 700–800 K suggests the presence of surface Co species with different degree of interaction with the support, possibly due to the reduction of cobalt silicate species formed during the TPR experiments by reaction of highly dispersed CoO with the silica support. As shown in Fig. 1, the Co-Pt/SiO₂ bimetallic catalysts can be reduced at a much lower temperature than Co/SiO₂. The two main reduction peaks of Co-Pt/SiO₂ decrease to about 400 K and 560 K, respectively, and the Co-Pt/SiO₂ catalysts become completely reduced at temperatures below 623 K.

On the other hand, Cu/SiO₂ and Cu-Pt/SiO₂ exhibit narrow and intense reduction peaks at 610 K and 600 K, respectively. The peak temperatures and profile shapes are consistent with previous work of TPR of pure CuO [33] and Cu/SiO₂ [34]. The TPR profiles indicate that all the catalysts, except monometallic Co, were completely reduced at 623 K. Previous work [35], by the H₂-TPR of the reference sample of mechanical mixture of 20 wt%CuO and 80 wt%SiO₂, has shown that the calculated degree of reduction of 10.0 wt%Co–1.2 wt%Pt/SiO₂ was 94%, indicating a complete reduction of the bimetallic catalysts. In addition, the catalytic evaluation was performed for Co/SiO₂ reduced at 623 K, 723 K, and 823 K, with the 723 K sample showing the highest activity. The Co catalyst should not be completely reduced at 623 K from the TPR of Co/SiO₂, whereas the Co metal particles would agglomerate when reduced at 823 K, both of which should lead to a lower activity. Therefore, the Co/SiO₂ catalyst was reduced at 723 K in the current work.

Table 1
CO chemisorption results and particle size distributions from TEM measurements.

Catalyst	CO uptake ($\mu\text{mol g}^{-1}$)	Particle size distribution statistics		
		Median diameter (nm)	Average diameter (nm)	Standard deviation in diameter (nm)
Co-Pt/SiO ₂	29.4	1.9	2.0	0.5
Cu-Pt/SiO ₂	8.8	2.5	2.6	0.5
Pt/SiO ₂	16.7	2.5	2.6	0.7
Co/SiO ₂	3.8	–	–	–
Cu/SiO ₂	1.1	–	–	–

Table 2
Results of Pt L_{III}-edge EXAFS fitting.

Catalyst	Pt/SiO ₂	Co-Pt/SiO ₂	Cu-Pt/SiO ₂
N(Pt-Pt)	9.1 ± 0.5	4.2 ± 1.0	3.0 ± 0.7
N(Pt-3d)	–	3.7 ± 0.5	8.1 ± 0.6
R(Pt-Pt) (Å)	2.75 ± 0.01	2.72 ± 0.01	2.68 ± 0.01
R(Pt-3d) (Å)	–	2.56 ± 0.01	2.60 ± 0.01
σ^2 (Pt-Pt) (Å) ²	0.006 ± 0.001	0.006 ± 0.001	0.006 ± 0.001
σ^2 (Pt-3d) (Å) ²	–	0.006 ± 0.001	0.009 ± 0.001

3.2. CO chemisorption measurements

The CO uptake values are listed in Table 1. The CO uptake for the Co-Pt/SiO₂ bimetallic catalyst is 29.4 $\mu\text{mol g}^{-1}$, higher than the sum of the two corresponding monometallic catalysts. However, the CO uptake value for the Cu-Pt/SiO₂ is less than the sum of the two monometallic catalysts. The CO uptake values on Cu/SiO₂ is less than 2 $\mu\text{mol g}^{-1}$, similar as the adsorption of CO on SiO₂ support itself [36], suggesting that the adsorption of CO on Cu/SiO₂ is negligible at 308 K.

3.3. TEM

High angle annular dark field (HAADF) TEM images and particle size distributions are shown in Fig. 2. Particle size distributions were calculated by measuring particle diameters in several different images for each catalyst using the software ImageJ and are summarized in Table 1. The dominant particle size in each catalyst appears to be the smaller particles ranging in diameter from approximately 1 nm to 4 nm. The average diameter is 2.0 nm for Co-Pt/SiO₂, and 2.6 nm for Cu-Pt/SiO₂ and Pt/SiO₂.

3.4. EXAFS

Fig. 3(a) shows the Pt L_{III}-edge X-ray absorption near-edge structure (XANES) spectra of the three catalysts before and after reduction, along with the spectra of the Pt foil for reference. Examining the Pt L_{III}-edge XANES reveals information regarding the oxidation state of the samples [37]. The XANES in Fig. 3(a) shows that before reduction in H₂ the catalysts exhibit large white-line peaks that disappear after reduction. All of the Pt L_{III}-edge spectra after reduction are similar to the Pt foil, indicating that the Pt has been fully reduced in the bimetallic catalysts.

Fig. 3(b) presents the Fourier transformed (R-space) experimental data after reduction and the fits obtained using FEFF6 [30]. The results from the fitting procedure are summarized in Table 2. In the bulk phase, Co and Pt have first nearest neighbor distances of 2.506 Å (Co-Co) and 2.774 Å (Pt-Pt). In the case of Pt-3d (3d = Co, Cu) bimetallic catalysts the first nearest neighbor distance should be an intermediate value between the two monometallic distances. As shown in Table 2, the Pt-Co distance falls between the bulk Co-Co and Pt-Pt distances, confirming the formation of Pt-Co bimetallic bonds. A similar trend is observed for Cu-Pt/SiO₂. Also, good fits to the Pt L_{III}-edge data could only be obtained by including both Pt-Pt and Pt-3d contributions in the model, which strongly suggests that bimetallic bonds are present in the bimetallic nanoparticles.

In addition to the Pt-3d interatomic distances, the Pt-3d coordination numbers can also be used to identify the presence of bimetallic bonds and measure the extent of bimetallic formation in the catalyst particles. As listed in Table 2, the Co-Pt and Cu-Pt coordination numbers are 3.7 and 8.1, respectively, confirming the presence of bimetallic bonds. The comparison also suggests that the extent of bimetallic formation is less in Co-Pt/SiO₂ than in Cu-Pt/SiO₂.

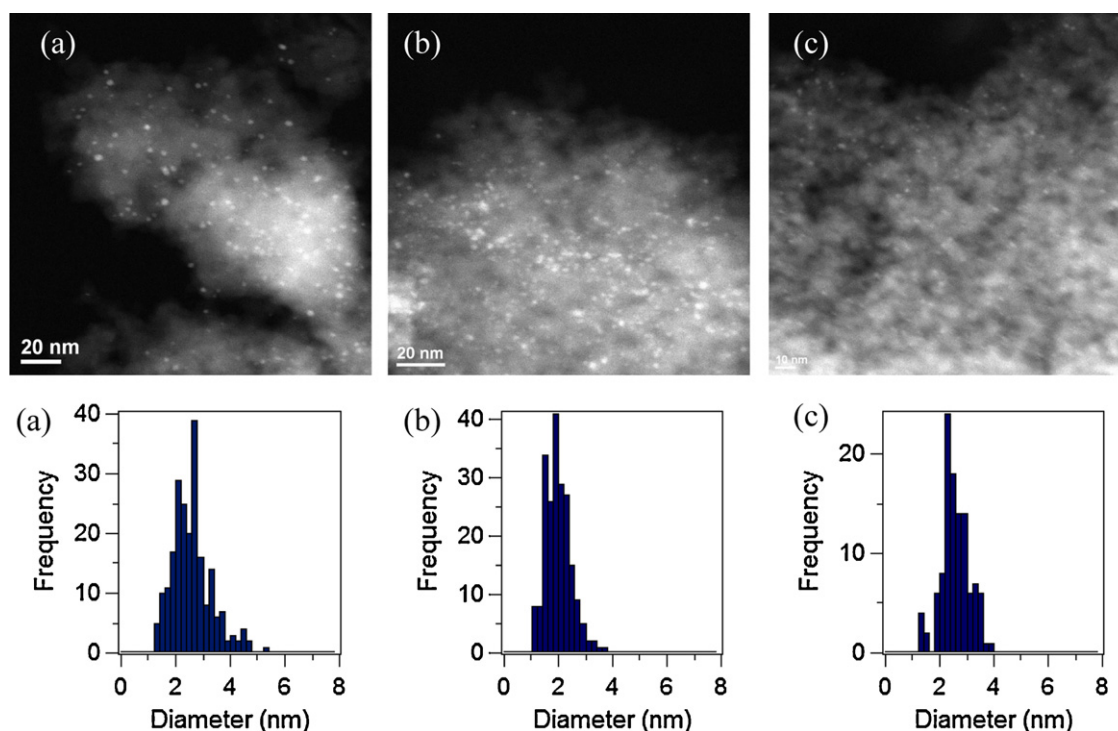


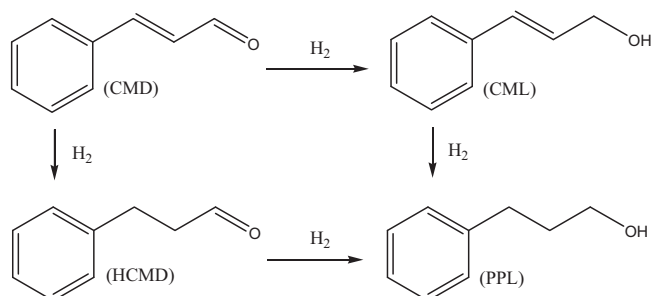
Fig. 2. TEM images and particle size distributions for (a) Pt/SiO₂, (b) Co-Pt/SiO₂ and (c) Cu-Pt/SiO₂.

3.5. Catalytic evaluation

The hydrogenation of CMD involves the parallel and consecutive reduction of two functional groups, C=C and C=O bonds. The products obtained were CML, hydrocinnamaldehyde (HCMD), and 3-phenylpropanol (PPL). In the current work no other side products were detected. Hence, the reaction pathways involved are believed to be those shown in Scheme 1.

The conversion of CMD and generation of products as functions of reaction time are displayed in Fig. 4. The conversion of CMD after 6 h on Co-Pt/SiO₂ bimetallic catalysts is up to 65%, three times higher than that on the corresponding monometallic catalysts. As the reaction time increases, the selectivity to CML decreases slightly. In contrast, Co/SiO₂ shows poor performance in terms of both activity and product selectivity, yielding nearly equal amounts of the semi-hydrogenated products, CML and HCMD.

To make a more quantitative comparison, the hydrogenation rate was quantified by fitting a first-order rate equation to the consumption of CMD, as listed in Table 3. The hydrogenation rate over Co-Pt/SiO₂ is 1.74 h⁻¹ g⁻¹, much higher than the sum of that over monometallic Co/SiO₂ and Pt/SiO₂. Because Co-Pt/SiO₂ showed much higher hydrogenation activity than Cu-Pt/SiO₂, we chose Co-Pt as the model bimetallic system to demonstrate the effect of



Scheme 1. Proposed schemes of cinnamaldehyde hydrogenation.

Table 3

Performance of the catalysts in terms of product selectivity at 20% conversion of cinnamaldehyde.

Catalyst	k (h ⁻¹ g ⁻¹)	Time required (h)	Product selectivity (%)			$S_{(C=O)/(C=C)}^a$
			CML	HCMD	PPL	
Co-Pt/SiO ₂	1.74	1.4	76	9.5	15	3.74
Co/SiO ₂	0.40	5.6	52	42	5.9	1.23
Pt/SiO ₂	0.28	8.8	70	29	1.7	2.34

^a The ratio of C=O bond hydrogenated (CML + PPL) to C=C bond hydrogenated (HCMD + PPL).

bimetallic formation on the hydrogenation selectivity. Typically the selectivity is compared at a similar conversion [9]. Therefore, the time required for 20% conversion of CMD was estimated from Fig. 2, and then used to obtain the product selectivity and the ratio of C=O to C=C hydrogenated, as listed in Table 3. The ratio of C=O to C=C hydrogenation is around 1 over Co/SiO₂, suggesting poor selectivity. In comparison, the ratio over Co-Pt/SiO₂ is 3.74. Comparing with Pt/SiO₂, the Co-Pt/SiO₂ shows higher selectivity to CML and lower selectivity to HCMD, indicating that Co-Pt/SiO₂ selectively hydrogenates the C=O bond rather than the C=C bond.

The performances of the Co-Pt and Cu-Pt catalysts in terms of conversion and selectivity after 2 h reaction time are compared in Table 4. The Co-Pt/SiO₂ and Cu-Pt/SiO₂

Table 4

Performance of the catalysts in terms of cinnamaldehyde conversion and product selectivity after 2 h reaction time.

Catalyst	Conversion (%)	Product selectivity (%)			$S_{(C=O)/(C=C)}$
		CML	HCMD	PPL	
Co-Pt/SiO ₂	28.6	78	8.8	14	4.02
Co/SiO ₂	7.9	58	38	4.4	1.45
Pt/SiO ₂	4.8	62	36	2.3	1.68
Cu-Pt/SiO ₂	10.7	35	60	5.2	0.61
Cu/SiO ₂	0	–	–	–	–

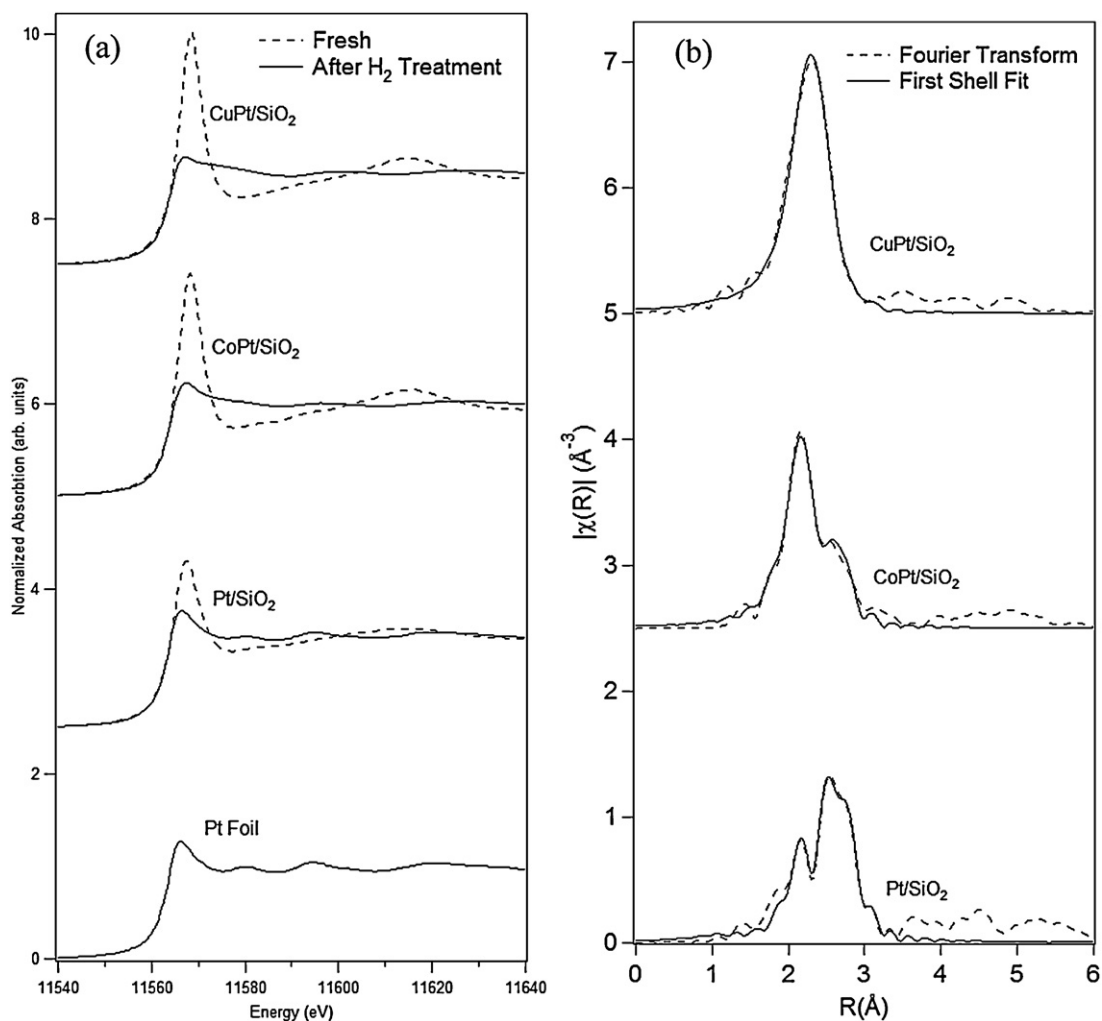


Fig. 3. (a) Normalized absorption of Pt L_{III} -edge XANES spectra of the three catalysts and a Pt foil before and after reduction; (b) Fourier transformed (magnitude) k^2 -weighted EXAFS function ($\chi(k)$) of Pt L_{III} -edge after reduction data (dashed lines) and first shell fits (solid lines).

catalysts show different hydrogenation activity and selectivity. In general, the catalytic activity follows the order of $\text{Co-Pt/SiO}_2 > \text{Cu-Pt/SiO}_2 > \text{Co/SiO}_2 > \text{Pt/SiO}_2$, while the selectivity to CML shows the trend of $\text{Co-Pt/SiO}_2 > \text{Pt/SiO}_2 > \text{Co/SiO}_2 > \text{Cu-Pt/SiO}_2$. The conversion of CMD over Cu-Pt/SiO_2 is higher than that over Pt/SiO_2 , and the Cu-Pt/SiO_2 prefers to hydrogenate the $\text{C}=\text{C}$ bond compared with Pt/SiO_2 . The Cu/SiO_2 shows no hydrogenation activity for the CMD.

4. Discussion

The results presented above demonstrate that Co-Pt and Cu-Pt bimetallic catalysts exhibit much higher hydrogenation activity than the corresponding monometallic catalysts, with Co-Pt showing much higher selectivity toward $\text{C}=\text{O}$ bond hydrogenation and Cu-Pt being more highly selective toward $\text{C}=\text{C}$ bond hydrogenation.

As indicated from the EXAFS results in Table 2, a significant fraction of the Pt atoms in the bimetallic catalysts are surrounded by Co or Cu atoms to form Co-Pt or Cu-Pt bimetallic bonds. In addition, the bimetallic catalysts can be reduced more easily than the monometallic Co or Cu catalysts, as demonstrated by the H_2 -TPR results in Fig. 1. The formation of the Co-Pt and Cu-Pt bimetallic catalysts should be responsible for the enhanced hydrogenation activity as compared to that of the corresponding monometallic catalysts.

It is also well established that an increase of metal particle size favors the selectivity to CML; the effect is particularly pronounced with particle larger than 2–3 nm [9,38,39]. This trend can be attributed to a steric effect whereby the planar CMD molecule cannot adsorb parallel to a flat metal surface because of the steric repulsion of the aromatic ring. By tilting away from the metal surface, the CMD molecule facilitates end-on adsorption and the $\text{C}=\text{C}$ bond is protected and hence the selectivity to CML is improved. However, the metal particle size alone cannot account for the different selectivity over Co-Pt and Cu-Pt bimetallic catalysts. As listed in Tables 1 and 4, the Co-Pt/SiO₂ catalyst, with metal particle size smaller than Pt/SiO₂, shows higher selectivity to CML. Furthermore, the Cu-Pt/SiO₂ and Pt/SiO₂ catalysts, possessing a similar metal particle size of 2.6 nm, show a significantly different selectivity trend. Therefore, the slight difference of the metallic particle size cannot account for the different selectivity trend of the two bimetallic catalysts.

As supported by the CO chemisorption measurements, the increase in the number of active sites on the Co-Pt/SiO₂ should partially contribute to the enhanced hydrogenation activity as compared to the monometallic catalysts. However, the surface active sites alone cannot explain the higher hydrogenation activity on the Cu-Pt/SiO₂, which has a lower CO uptake value than Pt/SiO₂. Therefore, it is necessary to understand the roles of Co and Cu on the activity/selectivity from the point of electronic modification, as discussed below.

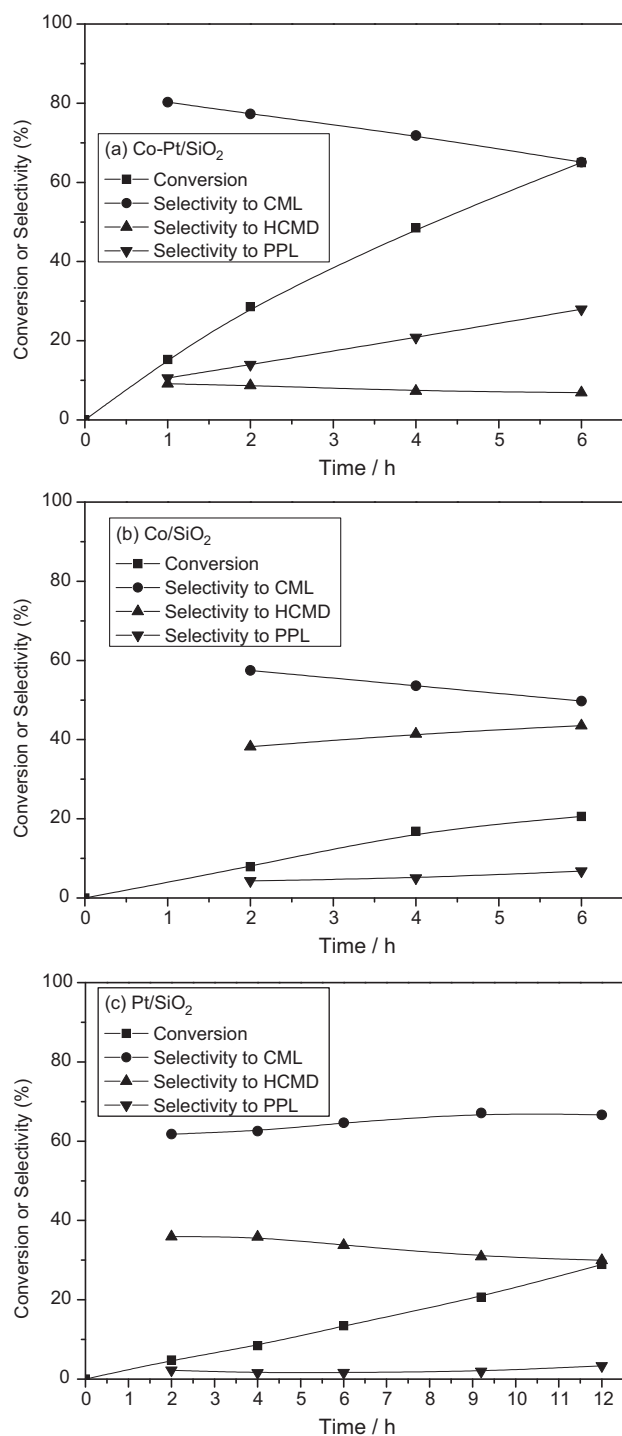


Fig. 4. Conversion of cinnamaldehyde (CMD) and generation of products as a function of reaction time over (a) Co-Pt, (b) Co and (c) Pt catalysts. Reaction conditions: 353 K, 3 mL CMD, 27 mL isopropanol (solvent), 4 MPa H₂, catalyst amount: 100 mg.

Previous work shows bimetallic surfaces that weakly bind atomic hydrogen and alkenes display greater hydrogenation activity [22]. This weak interaction between the surface and the adsorbates allows for novel, low-temperature hydrogenation to occur. Recently, Murillo et al. performed DFT and experimental studies to investigate the trend in C=C and C=O bond hydrogenation of acrolein, CH₂=CH-CH=O, on different bimetallic surface structures [19]. Selective hydrogenation of the C=O bond to produce 2-propenol (CH₂=CH-CH₂-OH) occurs on Pt-Co-Pt(111) as a result of the comparable binding strengths of the di-σ-C-C

and di-σ-C-O bonding configurations, with the latter favoring the C=O hydrogenation pathway [19]. Recent studies by FTIR spectroscopy of adsorbed CO and XPS on supported bimetallic catalysts have shown that after reduction, the surface of Co-Pt and Cu-Pt catalysts are composed of primarily Pt atoms [27,40], suggesting that the bimetallic nanoparticles may more closely resemble the Pt-terminated configurations from surface science studies [19]. As described in detail previously [19,22], the presence of subsurface Co and Cu modifies the electronic properties of surface Pt, leading to the low temperature hydrogenation of the C=O bond of unsaturated oxygenates. Furthermore, DFT calculations [41] and experimental verification [42] show that the Pt-terminated Pt-Co structure is preferred over Co-terminated Co-Pt-Pt in the presence of adsorbed hydrogen. Therefore, in the current work one can conclude that the enhanced hydrogenation activity observed over Co-Pt/SiO₂ and Cu-Pt/SiO₂ could be due to the presence of Pt-terminated bimetallic structures.

Additionally, both the hydrogenation activity and selectivity toward the C=O bond in CMD are much higher in Co-Pt/SiO₂ than over Cu-Pt/SiO₂. This is consistent with surface science studies by Murillo et al. [19] on acrolein hydrogenation, which shows that the activity and selectivity toward C=O bond hydrogenation on Pt-Co-Pt(111) is higher than that on Pt-Cu-Pt(111).

As reported by Gallezot and Richard [4], the selectivity of Pt toward C=O bond hydrogenation would be promoted with electropositive metal atoms. The electropositive metal acts as an electron-donor ligand that increases the electron density on Pt, thus decreasing the binding energies, particularly that of the C=C bond, favoring the hydrogenation of the C=O bond with respect to the C=C bond. This effect has been studied in detail theoretically by Delbecq and Sautet [43] on a model bimetallic surface Fe₂₀Pt₈₀(111), where the Fe atoms were located in the second layer. Calculations showed that the electropositive metal promoters acted as an electron-donating ligand, increasing the electron density on the surface platinum atoms. It is possible that such effect also plays a role in the selective hydrogenation of the C=O bond of CMD over the Co-Pt and Cu-Pt bimetallic catalysts. More detailed DFT calculations would be needed to further understand the mechanisms for the selective hydrogenation of CMD.

5. Conclusions

The current work extends the hydrogenation of monocarbonyl compounds to that of α,β-unsaturated aldehydes on silica supported Co-Pt and Cu-Pt bimetallic catalysts. Results from H₂-TPR studies show that the presence of Pt facilitates the reduction of 3d metals (Co or Cu). Pulse CO chemisorption measurements show that Co-Pt possesses significantly higher CO chemisorption capacity compared to monometallic catalysts. TEM and EXAFS measurements provide additional information on the metallic particle size distribution and the formation of bimetallic bonds. The reactor studies show that Co-Pt and Cu-Pt bimetallic catalysts exhibit significantly higher hydrogenation activity than the corresponding monometallic catalysts, and Co-Pt shows much higher selectivity toward C=O bond hydrogenation than Cu-Pt, consistent with previous surface science studies on the C=C and C=O bond hydrogenation of acrolein. The current work demonstrates a similar trend between model surfaces and supported catalysts, suggesting the possibility of using the relevant surface science results to design bimetallic catalysts for selective hydrogenation.

Acknowledgements

This work was supported by the United States Department of Energy, Office of Basic Energy Sciences (DE-FG02-00ER15104). The

authors from the Peking University acknowledge support from the Major State Basic Research Development Program (grant no. 2011CB808702).

References

- [1] P. Mäki-Arvela, J. Hajek, T. Salmi, D.Y. Murzin, *Appl. Catal. A* 292 (2005) 1–49.
- [2] D. Loffreda, F. Delbecq, F. Vigne, P. Sautet, *Angew. Chem. Int. Ed.* 44 (2005) 5279–5282.
- [3] H.U. Blaser, C. Malan, B. Pugin, F. Spindler, H. Steiner, M. Studer, *Adv. Synth. Catal.* 345 (2003) 103–151.
- [4] P. Gallezot, D. Richard, *Catal. Rev. Sci. Eng.* 40 (1998) 81–126.
- [5] N.M. Bertero, A.F. Trasarti, B. Moraweck, A. Borgna, A.J. Marchi, *Appl. Catal. A* 358 (2009) 32–41.
- [6] Y. Li, Z.G. Li, R.X. Zhou, *J. Mol. Catal. A* 279 (2008) 140–146.
- [7] A. Borgna, B.G. Anderson, A.M. Saib, H. Bluhm, M. Havecker, A. Knop-Gericke, A.E.T. Kuiper, Y. Tamminga, J.W. Niemantsverdriet, *J. Phys. Chem. B* 108 (2004) 17905–17914.
- [8] W.Y. Yu, Y. Wang, H.F. Liu, W. Zheng, *J. Mol. Catal. A* 112 (1996) 105–113.
- [9] N. Mahata, F. Goncalves, M.F.R. Pereira, J.L. Figueiredo, *Appl. Catal. A* 339 (2008) 159–168.
- [10] H. Vu, F. Goncalves, R. Philippe, E. Lamouroux, M. Corrias, Y. Kihn, D. Plee, P. Kalck, *P. Serp, J. Catal.* 240 (2006) 18–22.
- [11] M. Chatterjee, Y. Ikushima, F.Y. Zhao, *New J. Chem.* 27 (2003) 510–513.
- [12] A.B. Merlo, B.F. Machado, V. Vetere, J.L. Faria, M.L. Casella, *Appl. Catal. A* 383 (2010) 43–49.
- [13] C.Y. Hsu, T.C. Chiu, M.H. Shih, W.J. Tsai, W.Y. Cheu, C.H. Liu, *J. Phys. Chem. C* 114 (2010) 4502–4510.
- [14] A.J. Plomp, D.M.P. van Asten, A.M.J. van der Eerden, P. Mäki-Arvela, D.Yu. Murzin, K.P. de Jong, J.H. Bitter, *J. Catal.* 263 (2009) 146–154.
- [15] H. Li, J. Liu, H.X. Yang, H.X. Li, *Chin. J. Chem.* 27 (2009) 2316–2322.
- [16] B.M. Reddy, G.M. Kumar, L. Ganesh, A. Khan, *J. Mol. Catal. A* 247 (2006) 80–87.
- [17] M.X. Zhu, X.Q. Wang, J.Y. Lai, Y.Z. Yuan, *Catal. Lett.* 98 (2004) 247–254.
- [18] R. Hirschl, F. Delbecq, P. Sautet, *J. Catal.* 217 (2003) 354–366.
- [19] L.E. Murillo, C.A. Menning, J.G. Chen, *J. Catal.* 268 (2009) 335–342.
- [20] J.H. Sinfelt, *Acc. Chem. Res.* 10 (1977) 15–20.
- [21] J.H. Sinfelt, *Acc. Chem. Res.* 20 (1987) 134–139.
- [22] J.G. Chen, C.A. Menning, M.B. Zellner, *Surf. Sci. Rep.* 63 (2008) 201–254.
- [23] R.Y. Zheng, Y.X. Zhu, J.G. Chen, *ChemCatChem* 3 (2011) 578–581.
- [24] W.W. Lonergan, X.J. Xing, R.Y. Zheng, S.T. Qi, B. Huang, J.G. Chen, *Catal. Today* 160 (2011) 61–69.
- [25] S.T. Qi, W.T. Yu, W.W. Lonergan, B.L. Yang, J.G. Chen, *ChemCatChem* 2 (2010) 625–628.
- [26] W.O. Oduro, N. Cailuo, K.M.K. Yu, H.W. Yang, S.C. Tsang, *Phys. Chem. Chem. Phys.* 13 (2011) 2590–2602.
- [27] W.W. Lonergan, D.G. Vlachos, J.G. Chen, *J. Catal.* 271 (2010) 239–250.
- [28] M. Newville, *J. Synchrotron Radiat.* 8 (2001) 322–324.
- [29] B. Ravel, M. Newville, *J. Synchrotron Radiat.* 12 (2005) 537–541.
- [30] J.J. Rehr, R.C. Albers, *Rev. Mod. Phys.* 72 (2000) 621–654.
- [31] E. van Steen, G.S. Sewell, R.A. Makhothe, C. Micklethwaite, H. Manstein, M. de Lange, C.T. O'Connor, *J. Catal.* 162 (1996) 220–229.
- [32] A. Martinez, C. Lopez, F. Marquez, I. Diza, *J. Catal.* 220 (2003) 486–499.
- [33] M.F. Luo, Y.J. Zhong, X.X. Yuan, X.M. Zheng, *Appl. Catal. A* 162 (1997) 121–131.
- [34] A.J. Marchi, D.A. Gordo, A.F. Trasarti, C.R. Apesteguia, *Appl. Catal. A* 249 (2003) 53–67.
- [35] S.L. Lu, W.W. Lonergan, Y.X. Zhu, Y.C. Xie, J.G. Chen, *Appl. Catal. B* 91 (2009) 610–618.
- [36] S.T. Qi, B.A. Cheney, R.Y. Zheng, W.W. Lonergan, W.T. Yu, J.G. Chen, *Appl. Catal. A* 393 (2011) 44–49.
- [37] A. Jentys, B.J. McHugh, G.L. Haller, J.A. Lercher, *J. Phys. Chem.* 96 (1992) 1324–1328.
- [38] S.C. Tsang, N. Cailuo, W. Oduro, A.T.S. Kong, L. Clifton, K.M.K. Yu, B. Thiebaut, J. Cookson, P. Bishop, *ACS Nano* 2 (2008) 2547–2553.
- [39] E.V. Ramos-Fernandez, J.M. Ramos-Fernandez, M. Martinez-Escandell, A. Sepulveda-Escribano, F. Rodriguez-Reinoso, *Catal. Lett.* 133 (2009) 267–272.
- [40] R.T. Mu, Q. Fu, H.Y. Liu, D.L. Tan, R.S. Zhai, X.H. Bao, *Appl. Surf. Sci.* 255 (2009) 7296–7301.
- [41] C.A. Menning, J.G. Chen, *J. Chem. Phys.* 130 (2009) 174709.
- [42] C.A. Menning, J.G. Chen, *J. Power Sources* 195 (2010) 3140–3144.
- [43] F. Delbecq, P. Sautet, *J. Catal.* 164 (1996) 152–165.